J. Mol. Biol. (1992) **226**, 239–250

A 500 ps Molecular Dynamics Simulation Study of Interleukin-1β in Water

Correlation with Nuclear Magnetic Resonance Spectroscopy and Crystallography

Indira Chandrasekhar[1], G. Marius Clore[2], Attila Szabo[2], Angela M. Gronenborn[2] and Bernard R. Brooks[1]

[1]*Molecular Graphics and Simulation Laboratory*
Division of Computer Research and Technology, Building 12A and

[2]*Laboratory of Chemical Physics, Building 2*
National Institute of Diabetes and Digestive and Kidney Diseases
National Institutes of Health, Bethesda, MD 20892, U.S.A.

(Received 18 September 1991; accepted 10 March 1992)

We report the results of a 500 ps molecular dynamics simulation of the cytokine interleukin-1β, a protein of 153 amino acids, immersed in a sphere of 3783 bulk water molecules with a radius of 33 Å. The simulation reproduces the amplitudes of the fast librational motions of the backbone N–H bonds determined from ^{15}N nuclear magnetic relaxation data, as well as the crystallographic *B*-factors. Moreover, this study suggests a molecular picture of the nature of the slow internal motions that have been inferred from nuclear magnetic resonance relaxation experiments. These experiments indicated that, in addition to fast motions common to all residues, 32 surface residues exhibit slow motions on the 400 ps to 5 ns time-scale. While the present simulation is not sufficiently long to provide a quantitative description of events on this time-scale, it is long enough to observe several large amplitude transitions that are likely candidates for these slow motions. Specifically, in many of these 32 residues, the N–H groups are hydrogen bonded and infrequent dihedral transitions cause the N–H vectors to jump between states with well-defined orientations. It is shown that the time course of the angular reorientational correlation functions of these residues calculated from the trajectory is a reflection of the random times at which these infrequent jumps happen to have occurred. Thus, while the rate of these transitions cannot be quantified, the simulated decay of these correlation functions is completely consistent with the physical picture in which the N–H vectors, in addition to fast librational motion, undergo large amplitude jumps between conformations stabilized by hydrogen bonds.

Keywords: interleukin 1β; molecular dynamics simulation; n.m.r. relaxation; X-ray *B*-factors

1. Introduction

Protein structure, function and dynamics are intimately linked. From a theoretical perspective molecular dynamics (MD†) simulations provide a means of analysing motion at the atomic level and of obtaining a physical description of protein behaviour (Karplus & McCammon, 1981; Levy *et al.*, 1981; Brooks *et al.*, 1988). From the experimental viewpoint internal dynamics of proteins can be explored in solution using nuclear magnetic resonance (n.m.r.) relaxation measurements (London, 1980; Lipari & Szabo, 1982*a*,*b*; Lipari *et al.*, 1982) and in the crystal from an analysis of Debye-Waller temperature factors (Fraunfelder *et al.*, 1979; Artymuik *et al.*, 1979; Sternberg *et al.*, 1979; Hartmann *et al.*, 1982; Westhof *et al.*, 1984; Tainer *et al.*, 1984). In this paper, the structure and dynamics of interleukin-1β (IL-1β), a protein of 153 amino acids and molecular weight $17{\cdot}4 \times 10^3$, are investigated by a 500 ps MD simulation in water and correlated with recent n.m.r. spectroscopic (Clore *et*

† Abbreviations used: MD, molecular dynamics; n.m.r., nuclear magnetic resonance; IL-1β, interleukin-1β; r.m.s., root mean square; a.s.a., accessible surface area; NOE, nuclear Overhauser effect.

0022–2836/92/130239–12 $03.00/0

al., 1990*a*, 1991; Clore & Gronenborn, 1991) and crystallographic (Finzel *et al.*, 1989; Priestle *et al.*, 1989; Veerapandian *et al.*, 1992) data. IL-1β is of considerable biological interest, as it plays a central role in the immune and inflammatory responses (Oppenheim *et al.*, 1986; Dinarello & Savage, 1989). The primary goal of the present molecular dynamics study is to provide a physical basis for the nature of slow internal motions inferred from the n.m.r. relaxation behaviour of the protein (Clore *et al.*, 1990*a*,*b*).

The internal backbone dynamics of IL-1β have been characterized in solution using ^{15}N n.m.r. relaxation measurements and the behaviour of the residues falls into three distinct classes (Clore *et al.*, 1990*a*). Class 1 residues undergo fast motions on a time-scale of less than 20 ps. Class 2, which consists of 32 residues, exhibits additional slow motions in the range 400 ps to 5 ns. Both of these internal relaxations take place faster than the overall rotational correlation time of 8·3 ns. There is also a third class of 42 residues (class 3) that move on a time-scale much slower than the rotational correlation time and involve chemical exchange between different conformational states with distinct ^{15}N chemical shifts. It has been suggested that the internal motions of class 2 residues can be explained by a simple model in which the fast motion involves axially symmetric diffusion within a cone and the slow motion consists of jumps between two cones (Clore *et al.*, 1990*a*,*b*). The physical nature, however, of these motions was unresolved.

In this study, IL-1β is immersed in a sphere of 3783 bulk water molecules with a radius of 33 Å, which provides a shell of water 14 Å (1 Å = 0·1 nm) thick about the protein. The results of a 500 ps MD simulation of this system are compared with n.m.r. relaxation data and crystallographic Debye-Waller temperature factors. To our knowledge, this study represents the longest dynamics simulation of a protein in water that has been reported. Analysis of the protein trajectory suggests that the dynamics of the 32 residues belonging to class 2 are indeed distinct. Most of these residues are exposed on the surface and undergo large-amplitude motions. Surface exposure is in general correlated with large atomic fluctuations in the MD simulation, high Debye-Waller temperature factors in the X-ray structures and a greater error in the co-ordinates of the solution structure. The calculated angular reorientation correlation functions of the 32 N–H vectors of class 2 are distinguished by the presence of slow components to the decay, varying by several orders of magnitude from the fast decay experienced by all the residues. These components are shown to result from infrequent dihedral transitions that reorient the N–H vectors. On the time-scale of the simulation, certain of the mobile surface residues from class 1 and class 3 display similar behaviour to class 2. In particular one of the flexible loops, loop 3, which is dominated by residues of class 1, undergoes significant fluctuations. Unlike the other loops from class 2, however, it is not stabilized by hydrogen bonds and does not have a distinct secondary structure. The N–H vectors in this region fluctuate in a seemingly random manner, with the dihedral angles responsible for the fluctuations occupying a wide range of states, as opposed to the oriented transitions between hydrogen-bonded states that are seen in regions dominated by class 2 residues.

2. Methods

(a) *The initial setup*

The initial positional co-ordinates for the simulation were taken from the X-ray structure determined by Finzel *et al.* (1989; PDB accession number, 1I1B: notation in this paper, Xray1). These crystal co-ordinates were the earliest deposited in the Protein Data Bank (Bernstein *et al.*, 1977) and were available prior to the solution structure (Clore *et al.*, 1991). The first 3 residues of the protein, namely Ala, Pro and Val, are undefined in this structure and only 150 residues were included in the simulation. For residues with multiple occupancy factors (Lys63, Glu64 and Lys65), the positions with the highest occupancy were chosen. The side-chains of Lys93 and Lys94 are disordered in the crystal and were built in an extended conformation. The polar hydrogen atoms in the protein were added using the HBUILD (Brünger & Karplus, 1988) routine of CHARMM, yielding 1481 protein atoms. The 83 water molecules of crystallization were represented using a modified, flexible form of the TIP3P water model (Jorgensen *et al.*, 1983; Reiher, 1985). The initial setup consisted of 1730 atoms and was implemented on Apollo workstations.

All the initial setup and analysis were performed with CHARMM (Brooks *et al.*, 1983). The potential energy function used in the simulation has been described in detail (Brooks *et al.*, 1983). The energy parameters were obtained from the polar-hydrogen parameter set, PARAM19 (Reiher, 1985). The electrostatic interactions were calculated with a Coulomb potential and a dielectric constant of 1. They were truncated using a shifted potential (Brooks *et al.*, 1983) with a 11 Å cutoff, a value that has been shown to yield similar results to simulations done without a cutoff (Loncharich & Brooks, 1989). The van der Waals' interactions, represented by a Lennard-Jones potential, were also cut off at 11 Å. During dynamics, the non-bond list was updated every 20 steps using a 12 Å cutoff. The 1–4 electrostatic interactions were scaled to 0·4 of their value and the 1–4 Lennard-Jones interactions involving tetrahedral carbons were reduced (Reiher, 1985).

First, the protein was subjected to 100 steps of steepest descent minimization followed by 500 steps of adapted-basis Newton-Raphson minimization in the presence of strong harmonic restraints on the heavy atoms. By this procedure, short contacts in the protein were relieved and the system was allowed to relax while preserving the overall conformation. At this stage, the mass-weighted r.m.s. deviation from the input crystal co-ordinates was 0·037 Å for the backbone atoms and 0·042 Å for the protein heavy atoms. The minimized protein was immersed in a 33 Å radius sphere of 4799 water molecules selected from an equilibrated box of flexible TIP3P water molecules (Jorgensen *et al.*, 1983; Reiher, 1985). Water molecules within 2·7 Å of the protein were deleted, resulting in 3783 bulk water molecules. There are a total of 13,079 atoms in the final system. The system is roughly

25% protein by volume with a hydration shell of approximately 14 Å. The bulk water was allowed to relax around the protein during 400 steps of steepest descent minimization in the presence of small harmonic restraints on the protein heavy atoms. The resultant mass-weighted r.m.s. deviations from the input crystal for the backbone and the heavy atoms were 0·170 Å and 0·287 Å, respectively. This structure was used to provide the starting coordinates for the dynamics simulation.

(b) *The dynamics simulation*

The 500 ps MD trajectory was generated using the program GEMM on the STAR Technologies ST-100 array processor (Brooks, 1987). An integration time step of 0·001 ps was used. The first 10 ps of the simulation constitute the heating and early equilibration phases. At this stage, random velocities were assigned in accord with a Maxwell-Boltzmann distribution for temperatures increasing from 100 K to 300 K in steps of 100 K. In the final 8000 steps of this run, the velocities were assigned at 300 K. This was followed by a 10 ps equilibration phase during which the velocities were rescaled whenever the temperature fluctuated beyond a 10 K window. No further rescaling of velocities was required in that the temperature remained constant. As a precaution against instabilities from inadequate equilibration, the first 10 ps of the production run were not included in the analysis: the analysis run of 470 ps followed. For a system of this size with a 12 Å cutoff, 500 ps of simulation takes approximately 900 h of CPU time on a dedicated ST-100.

(c) *Solvent-accessible surface area calculations*

A solvent-accessible surface area (a.s.a) calculation measures the exposure of a specified region of a macromolecule (Lee & Richards, 1971; Shrake & Rupley, 1973). A probe radius of 1·4 Å was used (Lee & Richards, 1971) and the radii for the different atoms were set according to the Shrake and Rupley group radii with the hydrogen atoms not explicitly considered (Shrake & Rupley, 1973).

(d) *Hydrogen bond analysis*

The hydrogen bond energy was evaluated using the following function:

$$V_{HB} = \varepsilon_{min}[2(r_{min}/r_{AD})^6 - 3(r_{min}/r_{AD})^4] \times \cos^2(\theta_{A-H-D}) sw(r^2_{AD}, r^2_{Hon}, r^2_{Hoff}) \quad (1)$$

(Brooks *et al.*, 1983), where A represents the acceptor, D the donor and H the hydrogen atom. The well-depth and distance at the potential minimum are given by ε_{min} in kcal/mol and r_{min} in Å, respectively, r_{AD} is the separation between A and D, and θ_{A-H-D} the angle A–H–D. The cutoffs for the switching function, $sw(r^2_{AD}, r^2_{Hon}, r^2_{Hoff})$, described by Brooks *et al.* (1983), were Hon = 4·0 Å and Hoff = 5·0 Å. The hydrogen bond list was cut off at 5·5 Å. It should be emphasized that no explicit hydrogen-bonding function was used during the simulation. The non-bonded, electrostatic interactions in the parameter set, PARAM19, have been refined to represent peptide hydrogen bonds accurately (Reiher, 1985).

(e) *The angular reorientation correlation function*

The angular reorientational correlation function describing the dynamics of an N–H bond is $\langle P_2(\hat{\mu}(0)\cdot\hat{\mu}(t))\rangle$ where $\hat{\mu}$ is a unit vector pointing along the N–H bond and $P_2(x) = (3x^2/2 - 1/2)$ is the second Legendre polynomial. These functions were calculated from a simulation of length T *via*

$$\langle P_2(\hat{\mu}(0)\cdot\hat{\mu}(t))\rangle = \frac{1}{T-t} \times \int_0^{T-t} d\tau\, P_2(\hat{\mu}(\tau)\cdot\hat{\mu}(t+\tau)). \quad (2)$$

The long time limit of this function is defined as the square of the generalized order parameter (S^2) and was obtained from the simulation using:

$$S^2 = \frac{1}{T^2}\int_0^T \int_0^T dt d\tau\, P_2(\hat{\mu}(\tau)\cdot\hat{\mu}(t+\tau)). \quad (3)$$

For trajectories of finite length that do not adequately sample conformation space, the long time limit calculated using eqn (2) will in general differ from the value obtained from eqn (3).

3. Results and Discussion

(a) *Structural analysis*

IL-1β consists primarily of β strands and β turns, and is depicted by a schematic diagram of the secondary structure elements in Figure 1 and by a series of snapshots of the backbone of IL-1β during the course of the MD simulation of Figure 2. The six-stranded barrel is made up of β strands β1, β4, β5, β8, β9 and β12. The 32 residues of class 2, characterized by a slow component to the ^{15}N relaxation, occur: (1) along the extended loops on the capped side of the β barrel, (2) in the shorter loops on its exposed side and (3) in one case in a β strand that forms part of the β barrel. Many of the class 2 residues are located in stretches of several amino acids that exhibit similar behaviour. Some of those that appear isolated (e.g. Gly22) may in fact have neighbouring residues belonging to the same class but the determination of their relaxation behaviour was prevented by severe resonance overlap (Clore *et al.*, 1990*a*). Ser17 and Gly22 flank the β strand, β2, and Leu26 forms the beginning of the adjacent strand, β3. These three residues, unlike most of the others of class 2, are relatively unex-

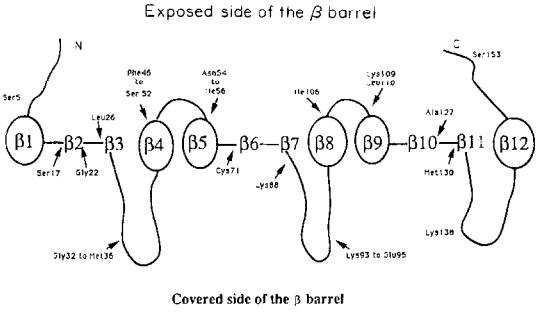

Figure 1. Schematic diagram of the secondary structural elements of IL-1β. The β strands are labelled and those that form part of the 6-stranded β barrel are represented as ellipses. The 32 residues of class 2 are shown in their approximate positions. These residues belong primarily to the extended loops on the capped side of the β barrel, to the shorter loops on its exposed side and, in one case, to a β strand that forms part of the β barrel.

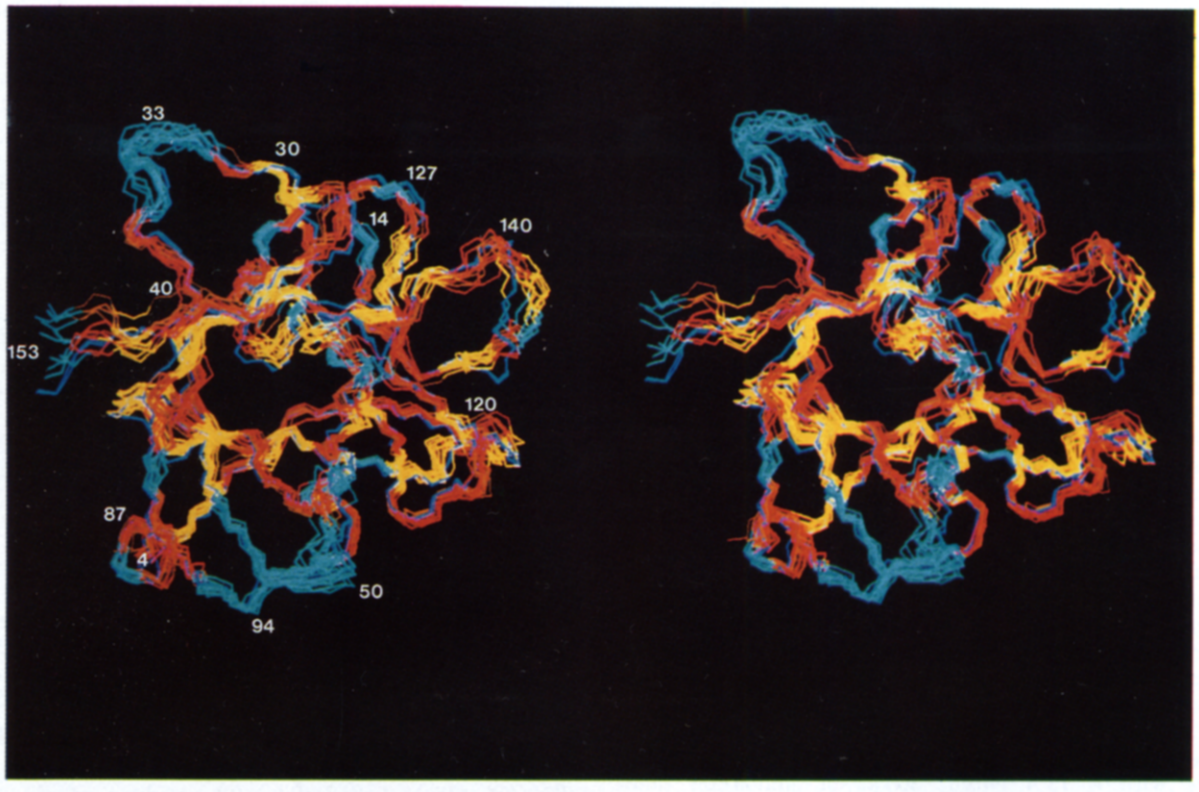

Figure 2. Snapshots of the backbone of IL-1β at 50 ps intervals during the course of the simulation. The 32 residues of class 2 are shown in turquoise, the 42 residues of class 3 in yellow and the rest in orange and red. The input crystal structure is shown in dark blue. The residues on the surface are flexible. Among the most mobile segments are loop 1 (Gln32 to Met36) shown in turquoise in the upper left-hand corner of the Figure and loop 3 (Lys138 to Leu143) on the right-hand side of the Figure.

posed. They occur on the side of the β barrel that is not capped by the extended loops (Fig. 2). Most of the residues of loop 1 (Leu31 to Gln39) belong to class 2. Residues Gln32 to Met36 form a short stretch of 3_{10} helix on the surface of the protein, linking strands β3 and β4. Phe46 to Glu50 and Ser52 form part of the antiparallel β barrel where the hydrogen-bonding pattern is perturbed to accommodate Pro57 of the neighbouring strand. Here the a.s.a. per residue is relatively high and the backbone atoms are exposed to the surface (Fig. 3); water molecules are implicated in bridging the strands β4 and β5 (Finzel *et al.*, 1989; Priestle *et al.*, 1989; Clore *et al.*, 1990*c*, 1991; Veerapandian *et al.*, 1992). There is a backbone hydrogen bond between Gln48 and Lys93 of the extended loop 2, which is maintained throughout the simulation. Asn53 to Ile56 form a type I turn linking strands β4 and β5, and are significantly exposed to the surface. The next residue of class 2, Cys71, is one of the seven buried, hydrophilic residues identified in the solution structure (Clore *et al.*, 1991). The backbone is involved in a stable hydrogen bond with Arg98 of loop 2, while the SH group hydrogen bonds with Ser114 in strand β9. Unlike those of the other residues of class 2, the amplitude of the fluctuation for Cys71 is small. Many of the residues of the second extended loop belong to class 2. Lys88 is the third residue of a type I β turn leading up to loop 2 and is well exposed. The portion of loop 2 between Lys93 and Glu96 forms a helix-like stretch. In solution, this region undergoes a slow conformational transition between a major and a minor form (Driscoll *et al.*, 1990; Clore *et al.*, 1990*a*). The region from Ile106 to Leu110 forms the turn between strands β8 and β9 on the exposed side of the β barrel and is accessible to the surface. The residues Ala127 and Met130 lie between strands β10 and β11. Lys138 belongs to the third extended loop, although none of the other residues of this highly flexible region of the protein belongs to class 2.

The residue-based relative fractional a.s.a. values for the heavy atoms are shown in Figure 3. In this, as in all the histograms that follow, the residues of class 2 are shown as filled bars, those of class 3 as hatched bars and the rest as open bars. There is a clear correlation between the exposed and flexible regions of IL-1β (Figs 2, 3 and 7). The surface exposure is similar in the simulated, in the solution and in the three crystal structures. The correlation coefficients between the five different structures are above 0·6 when the C-terminal residues, which display the maximum variation, are not included. The regions with the maximum backbone exposure are the extended loops, loop 1 (Leu31 to Gln39), part of loop 2 and the turn preceding it (Val85 to

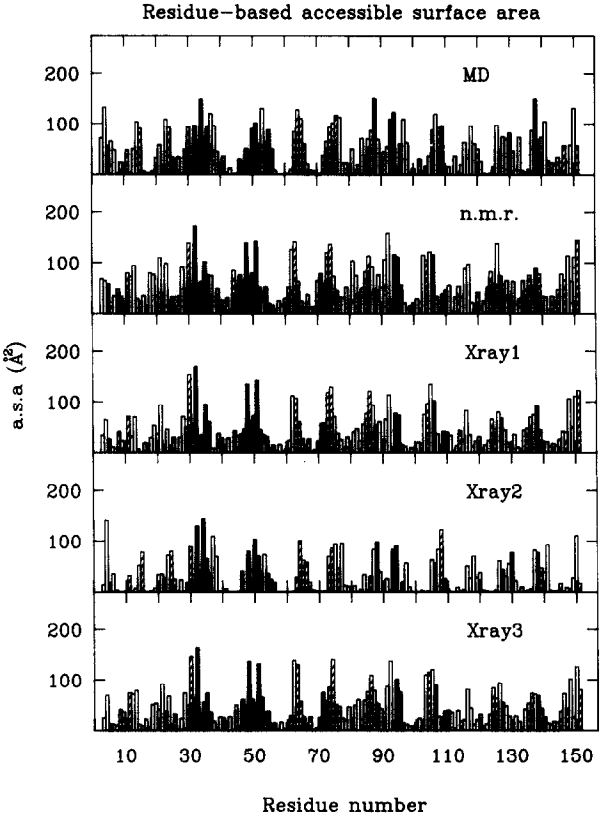

Figure 3. Solvent-accessible surface area for the individual residues. The 32 residues of class 2 are shown as filled bars, the 42 residues of class 3 as hatched bars and the remaining ones as open bars. This convention is used throughout. Most of the residues of class 2 are well exposed.

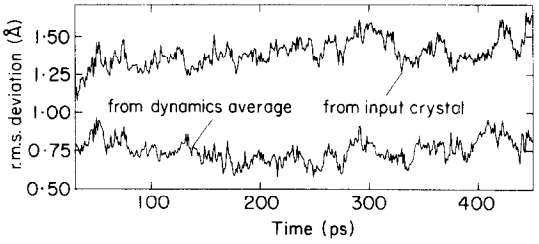

Figure 4. The r.m.s. deviations from the starting crystal co-ordinates (Finzel *et al.*, 1989) and the dynamics averaged structure as a function of time.

Met95), loop 3 (Thr137 to Ile143) and the β turn between strands β4 and β5 (Ser52 to Lys55). Loops 1, 2 and the β turn belong to class 2, with a slow component to the internal relaxation, while the N–H vectors of loop 3 experience only the fast relaxation (class 1).

(b) *Dynamics analysis*

The mass-weighted r.m.s. deviations of the protein backbone about the input crystal and the dynamics-averaged structures, respectively, are shown in Figure 4. The structures are aligned by least squares fitting the backbone atoms before evaluating the r.m.s. deviations, thus avoiding effects arising from rotational and translational drift during the simulation. The average backbone r.m.s. deviation from the input crystal co-ordinates (Finzel *et al.*, 1989) is 1·4 Å and about the dynamics averaged structure is 0·75 Å. Deviations on this scale are reasonably

Table 1

Atomic r.m.s. deviations between the various IL-1β structures, and correlation coefficients between the fluctuations of the backbone atoms from the MD simulation, the backbone atomic r.m.s. deviation about the mean co-ordinate positions for the solution n.m.r. structure and the backbone-averaged B*-factors from the three crystal structures*

	r.m.s. difference (Å)		Correlation coefficient	
	Backbone	Heavy atoms†	Backbone	Heavy atoms
MD *versus* n.m.r.	1·197	1·769	0·716	0·706
MD *versus* Xray1	1·176	1·647	0·694	0·735
MD *versus* Xray2	1·250	1·815	0·386	0·657
MD *versus* Xray3	1·148	1·685	0·626	0·726
n.m.r. *versus* Xray1	0·894	1·501	0·798	0·729
n.m.r. *versus* Xray2	0·878	1·619	0·649	0·662
n.m.r. *versus* Xray3	0·874	1·548	0·738	0·744
Xray1 *versus* Xray2	0·355	1·088	0·661	0·704
Xray1 *versus* Xray3	0·317	0·844	0·921	0·952
Xray2 *versus* Xray3	0·366	1·164	0·609	0·695

The notation of the structures is as follows: Xray1, Xray2 and Xray3 are the crystal structures of Finzel *et al.* (1989), Priestle *et al.* (1989) and Veerapandian *et al.* (1991), respectively (PDB accession numbers, 1I1B, 2I1B and 4I1B); n.m.r. is the restrained minimized mean n.m.r. structure (Clore *et al.*, 1991; PDB, accession number 6I1B); MD is the average structure of the 500 ps MD simulation.

† The mass-weighted r.m.s. deviation for the protein heavy atoms.

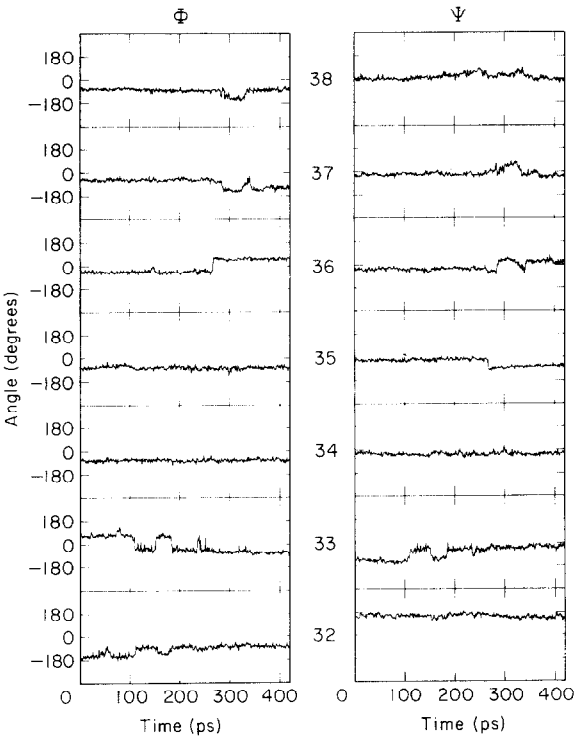

Figure 5. The dihedral angle transitions in the extended loop 1 (Gln32 to Gln36) as a function of time. The residue numbers are shown between the panels. Transitions between adjacent $\phi(i+1)$ and $\psi(i)$ angles are anti-correlated. The exception of this trend is the highly flexible Gly33, where the ϕ and ψ of the same residue are highly anti-correlated.

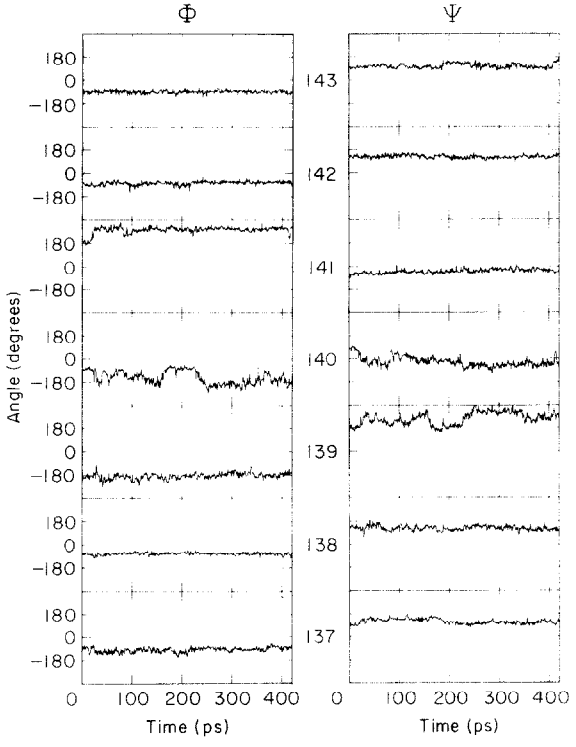

Figure 6. Dihedral angle transitions in loop 3 (Lys138 to Asn143) as a function of time. Although, the transitions are not as extensive as in loop 1, here too anti-correlated transitions between adjacent $\phi(i+1)$ and $\psi(i)$ are seen. The most flexible residue in this segment is Gly140. The residue numbers are shown between the corresponding panels for ϕ and ψ.

typical in protein simulations carried out in the presence of solvent (Brooks *et al.*, 1988; Loncharich & Brooks, 1990) and are significantly lower than results obtained from vacuum simulations. Also of interest (Table 1) is the observation that the backbone r.m.s. difference between the dynamics averaged structure and the restrained minimized mean n.m.r. structure (1·2 Å) is the same as that between the dynamics average structure and the three X-ray structures (1·2 ± 0·05 Å), and only slightly larger than that between the n.m.r. and X-ray structures (0·88 Å). (For comparison, the backbone r.m.s. difference is 0·35 ± 0·03 Å between the three X-ray structures and 0·41 ± 0·04 Å between the calculated n.m.r. structures.) There is considerable flexibility in the loop regions of the proteins as can be seen in Figure 2, which depicts snapshots of the structure at 50 ps intervals during the course of the MD simulation.

Transitions occur in the backbone dihedral angles of some of the flexible residues though most residues remain in their initial states. The transitions that take place are anti-correlated, preserving the overall fold of the protein after 500 ps of simulation. Concerted transitions take place in adjacent $\phi(i+1)$ and $\psi(i)$ angles, resulting in the type of crank-shaft motion seen in previous protein simulations (McCammon *et al.*, 1977; Levitt, 1983; Brooks *et al.*, 1988). The 3_{10} helical loop, loop 1, between Gln32 and Met36, which in the simulation has the largest fluctuations of the class 2 residues, undergoes a significant number of dihedral angle transitions (Fig. 5). Several transitions occur in Gly33. This residue is unusual in that its two backbone dihedral angles are themselves anti-correlated. Transitions take place between the gauche$^+$ and gauche$^-$ conformations for $\phi(33)$ and between the trans and gauche$^-$ for $\psi(33)$. These dihedral angles are in turn correlated with $\phi(32)$, which undergoes transitions between the trans and gauche$^-$ states. The adjacent dihedral angles of residues Asp35, Met36, Glu37 and Gln38 are anti-correlated and "jumps" between different states are seen (Fig. 5). Fluctuations in $\phi(38)$ and $\psi(38)$ take place simultaneously and are in turn anti-correlated with $\psi(37)$.

A number of dihedral transitions are also observed in loop 3 (Thr137 to Ile143) (Fig. 6). Anti-correlations are seen between the adjacent ϕ and ψ angles of Lys138, Gly139, Gly140 and Gln141. The most significant fluctuations involve the highly exposed Gly140. The dihedral angles $\psi(139)$, $\phi(140)$ and $\psi(140)$ do not undergo the two-site jumps seen in loop 1 but instead occupy a range of values. Gly140 and Gln141 belong to class 1 where the n.m.r. relaxation time is less than 20 ps. Of the remaining residues in the loop, Lys138 belongs to class 2, and Gly139 to class 3.

There are three hydrogen bonds along the 3_{10}

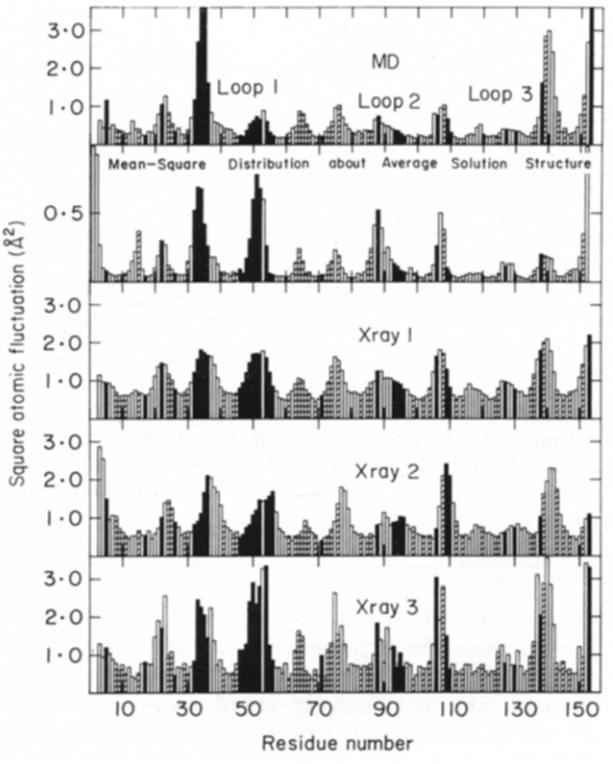

Figure 7. Comparison of the backbone square atomic fluctuations calculated from the MD simulation, the backbone atomic mean-square deviation about the average co-ordinate positions for the solution n.m.r. structure and the square atomic fluctuations obtained from the backbone crystallographic *B*-factors for the 3 crystal structures (the 3 lower panels). Note that the scale for the second panel from the top, showing the average square r.m.s. deviation of the individual n.m.r. structures about the mean co-ordinate positions, is three times smaller than that for the square atomic fluctuations.

helical loop, loop 1, between residues Met36(N)–Gly33(O), Met36(N)–Gln32(O) and Gln38(N)–Asp35(O). The first two are anti-correlated in the first 200 ps, the energy of one bond increasing when the other decreases and *vice versa*. Two of the hydrogen bonds, Met36(N)–Gly33(O) and Gln38(N)–Asp35(O), break during the course of the simulation and do not re-form. The breaking in this case is synonymous with the acceptor–donor distance going beyond the list cutoff of 5·5 Å. The residues of loop 2 have hydrogen bonds, characteristic of turns, that are stable throughout the course of the simulation. There is a stable hydrogen bond between the backbone atoms of Lys93 and Gln48. Experimental evidence suggests that residues in the vicinity of Lys93 undergo conformational transitions (Clore *et al.*, 1990*a*) and it is possible that this hydrogen bond would indeed fluctuate if the simulated sample time were much longer.

The third long loop, loop 3, is extremely flexible and undergoes large amplitude motion throughout the entire MD simulation. The experimental n.m.r. data, however, provide no evidence of ISN chemical exchange line broadening in this region indicative of motion in solution on a time-scale longer than the rotational correlation time (~8 ns). (Note that for this to occur the time scale of the motion cannot be in the fast exchange limit on the chemical shift scales.) This is the region of most pronounced discrepancy between the n.m.r. data and the simulation. In the MD simulation, the backbone atoms of loop 3 do not seem to form the series of hydrogen bonds that stabilize the other two loops, and its mobility is of a different nature from that of loops 1 and 2. In particular, the fluctuations of the dihedral angles and hence of the N–H vectors in loop 3 are more random and undirected, unlike those of loops 1 and 2 where the N–H vectors jump between oriented hydrogen-bonded states.

(c) *The atomic fluctuations or* B*-factors*

The three reported X-ray structures of IL-1β (Finzel *et al.*, 1989; Priestle *et al.*, 1989; Veerapandian *et al.*, 1992) crystallize in the same space group ($P4_3$) with almost identical cell dimensions (a = 55·0 Å, b = 55 Å and c = 77 Å) and the mass-weighted r.m.s. deviation between the respective protein backbones is ~0·4 Å (Table 1). Surprisingly, there are variations in the Debye-Waller temperature factors of the three crystals, possibly arising from differences in the respective crystallographic refinement procedures. Figure 7 shows a comparison of the square atomic fluctuations $\Delta\mathbf{r}^2$ obtained from crystal *B*-factors ($B = 8\pi^2\langle\Delta\mathbf{r}^2\rangle/3$) with the residue-averaged mean square atomic fluctuations derived from the MD simulation. The general trends are similar and in all cases correlate strongly with surface exposure (Figs 3 and 7). The tendency in the past has been to make specific residue-based comparisons between experimental *B*-factors and atomic fluctuations calculated from simulations (Levitt, 1983; Post *et al.*, 1986). Instead, we evaluate the correlation coefficients between the residue and backbone-averaged *B*-factors from the three (crystal, solution and calculated) structures (Table 1). The correlation between the crystallographic values and those derived from simulation lies in the same range as do the correlations between the different crystals. The lowest correlation is exhibited by the structure termed Xray2 (Priestle *et al.*, 1989), where the *B*-factors of the C-terminal residues are small (Fig. 7). An evaluation of the correlation coefficients without the last two residues dramatically improves the correlation; thus the correlation coefficient for Xray2 *versus* the simulation average structure increases from 0·386 to 0·666.

The mean-square deviation about the average backbone co-ordinate positions for the solution n.m.r. structures is also shown in Figure 7 (Clore *et al.*, 1991). This quantity measures the variations in the atomic co-ordinates consistent with the n.m.r. data and is significantly smaller than the *B*-factors. Regions with large *B*-factors in the crystal generally have a large r.m.s. deviation about the mean solution structure. The exposed regions exhibit the

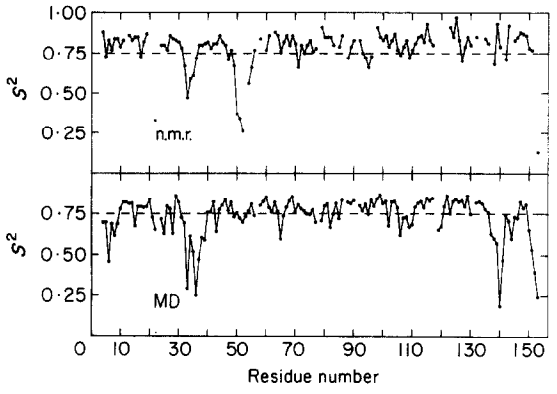

Figure 8. Comparison of the generalized square order parameter (S^2) obtained from ^{15}N n.m.r. relaxation experiments and from the MD simulation. The broken lines serve simply to guide the eye.

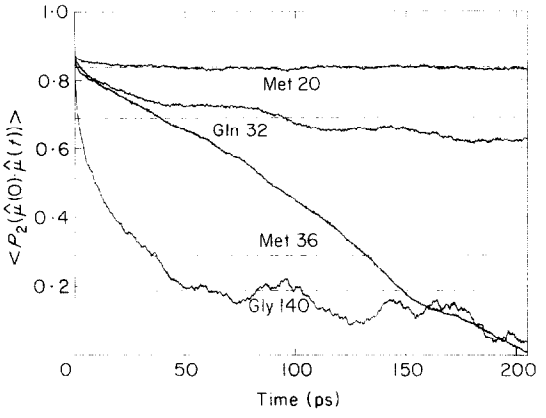

Figure 9. The angular reorientational correlation functions, $\langle P_2(\hat{\mu}(0)\cdot\hat{\mu}(t))\rangle$, for Met20 (class 1), for Gln32 and Met36 (class 2 from loop 1), and for Gly140 (class 1 from loop 3).

maximum variation (Figs 3 and 7). Of the regions with a large r.m.s. deviation in the solution structure, loop 1 (Leu31 to Gln39) and strand β4 (Phe46 to Ser52) have been found to undergo overall displacements of the secondary structural element, rather than experiencing local disorder (Clore *et al.*, 1991). Loop 3 is reasonably well determined although the region has relatively large *B*-factors and undergoes large fluctuations in the simulation. The correlation coefficients between the solution, crystallographic and simulation-based fluctuations are high and within the range of variation seen between the three crystal *B*-factors (Table 1).

The square atomic fluctuations evaluated from the simulation are in general lower than those derived from the crystal *B*-factors (Fig. 7). This is either because the available conformational space is not fully sampled by the 500 ps simulation or because the simulated atomic fluctuations do not take into account the inherent conformational microheterogeneity existing in the crystal (Fraunfelder *et al.*, 1979; Ichiye & Karplus, 1988). Reduced fluctuations are seen between Ser45 and Lys55, in the turns between Lys74 and Lys77 and between Glu105 and Leu110. The region from Val85 to Met95 (part of loop 2 and some preceding residues) contains residues that undergo conformational transitions (Clore *et al.*, 1990*a*) and is clearly not sampled completely by the simulation. On the other hand, the atomic fluctuations for the residues in loops 1 and 3 are much higher in the simulation than in the X-ray structures, possibly due to the fact that these surface residues are unconstrained in the simulation by the packing interactions of the crystal.

(d) *Generalized order parameters*

The generalized order parameter is a measure of the amplitude of angular motions. The generalized order parameters of the N–H vectors of 144 residues (excluding 7 prolines) evaluated from the MD trajectory using equation (3) are compared with those extracted from n.m.r. relaxation measurements (Clore *et al.*, 1990*a*) in Figure 8. For most of the residues the experimental squared order parameters, S^2, are close to 0·8, indicating that the motions are of relatively small amplitude. (Thus $S^2 = 0{\cdot}83$ corresponds to a cone with a semiangle of 20°). These are well reproduced by the simulation. In addition, there is qualitative agreement between simulation and experiment, in that both indicate that large amplitude motions occur in loop 1 (residues 32 to 36). The MD simulation, however, fails to detect the enhanced mobility of residues near 50 that is evident both from the n.m.r. and X-ray (see Fig. 7) results. It is possible that the trajectory is just too short to explore enough of this part of conformational space. It is more difficult to rationalize why the large amplitude fluctuations of loop 3 (residues 138 to 143) predicted by the MD simulation are not seen in the n.m.r. but are consistent with the X-ray temperature factors.

(e) *Angular reorientational correlation functions*

To gain insight into the nature of the dynamics, the angular correlation functions $\langle P_2(\hat{\mu}(0)\cdot\hat{\mu}(t))\rangle$ for the 144 N–H vector were evaluated up to 205 ps from a 420 ps segment of the trajectory using equation (2). It should be emphasized that the time course of these correlation functions is expected to be meaningful only for much shorter times (see, e.g. Zwanzig & Ailawadi, 1969; Allen & Tildesley, 1987; Pastor, 1992; and the analysis below). The results for four representative residues are shown in Figure 9. The broken lines correspond to S^2 calculated using equation (3). Met20 belongs to class 1, Gln32 and Met36 are class 2 residues in loop 1, while Gly140 is a class 1 residue in the middle of loop 3.

All the correlation functions exhibit an ultrafast subpicosecond decay to a value of about 0·85. Met20 decays a little further, stabilizing around 0·82, which is good agreement with S^2 calculated using equation (3). This behaviour is a classic example of what is expected for a residue undergoing small amplitude fast motions. The correlation function of

Gly140 also appears to be reasonably well converged. The amplitude, however, is much larger ($S^2 \sim 0{\cdot}2$) and the time-scale is somewhat faster. This behaviour is consistent with the fact that loop 3 appears to have no specific secondary structure in the MD simulation and that the dihedral angles that determine the orientations of the N–H vectors vary over a wide range of values. As mentioned above in section (d), the large amplitude motions in loop 3 predicted by the MD simulations are consistent with the X-ray results but not with the n.m.r. relaxation data.

Now consider the correlation function of Met36, a class 2 residue from loop 1. At first sight, it appears that, in addition to the ultrafast decay, there are large amplitude motions on the 100 ps time-scale reorienting the N–H vector of this residue. This, however, is not at all the case, and in fact the time course of this correlation function is an artefact resulting from incomplete sampling. There are two indications of this: first, the correlation function crosses the supposed long time limit indicated by the broken line; and second, rather than being exponential, the correlation function is virtually linear from 10 to 150 ps.

An examination of the MD trajectory shows that the N–H vector of Met36 undergoes a large change in orientation at about 270 ps. This is the result of concerted dihedral angle transitions and is evident from the time course of the ϕ backbone torsion angle of Met36 shown in Figure 5. Up to 270 ps the backbone amide of Met36 is hydrogen-bonded to the backbone carbonyl of Gly33. After this transition, the hydrogen bond switches to the backbone carbonyl of Gln32. The overall result is that the orientation of the N–H vector changes by about 105°.

A MD trajectory that contains only a single transition is clearly much too short to determine the rate of this process. Even though it is not meaningful in a statistical sense, such a trajectory can be used to calculate a correlation function using equation (2). Suppose that in a trajectory of length T there is a single transition at $t = t_0'$ in which a vector with orientation $\hat{\mu}_1$ jumps to a state where its orientation is $\hat{\mu}_2$. Using equation (2) it can readily be shown that:

$$\begin{aligned} \langle P_2(\hat{\mu}(0)\cdot\hat{\mu}(t))\rangle &= 1 - \frac{t}{T-t}(1-P_2(\cos\delta)) \\ & \qquad\qquad 0 \le t < t_0 \\ &= 1 - \frac{t_0}{T-t}(1-P_2(\cos\delta)) \\ & \qquad\qquad t_0 < t \le T/2, \end{aligned} \tag{4}$$

where $t_0 = \min(t_0', T-t_0')$ and δ is the angle between $\hat{\mu}_1$ and $\hat{\mu}_2$. According to this result the correlation function consists of two essentially linear segments with a break in slope at time t_0. In addition, equation (4) can even become negative for certain range of parameters! The correct correlation function for a two-site jump model, on the other hand, is always positive, decaying from unity to the squared generalized order parameter as a single exponential.

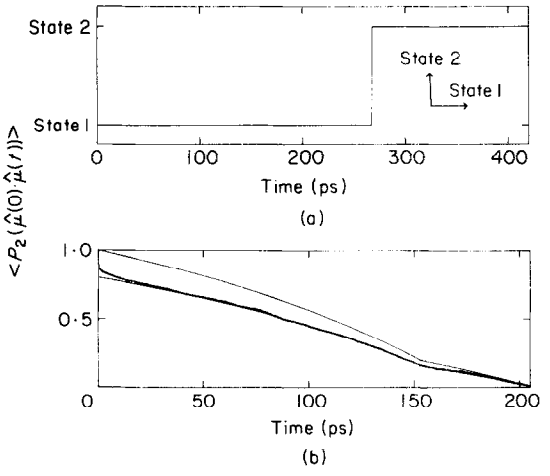

Figure 10. Comparison of the angular reorientational correlation function, $\langle P_2(\hat{\mu}(0)\cdot\hat{\mu}(t))\rangle$, for Met36 calculated from the MD simulation (thick line with "noise", (b)) with that (thin line starting at 1·0, (b)) calculated from the model trajectory shown in (a). This trajectory depicts a single transition between states 1 and 2 occurring at 270 ps, which reorients the N–H vector by ~105°. When the resulting correlation function is scaled by 0·8 to allow for ultrafast librational motion in the 2 states, it becomes virtually identical to the result calculated from the full MD trajectory.

An application of this result to Met36 is presented in Figure 10(a) represents a trajectory in which a single transition between states 1 and 2 occurs at about 270 ps. In Figure 10(b) we compare the correlation function calculated from the MD simulation (thick line with "noise") with that predicted by equation (4) with $\delta = 105°$ (thin line starting out at unity). The shapes of the curves are remarkably similar. In particular, both show an apparent change in the slope at $t_0 = 150$ ps ($t_0 = T - t_0' = 420 - 270$ ps). The MD correlation function, however, exhibits a very rapid initial decay due to librational motion of the N–H vector on the subpicosecond time-scale. Assuming that this motion is independent of the jump motion between the two states, one can easily incorporate this effect into the model calculation by multiplying equation (4) by the square of the librational order parameter. Multiplying the two-site jump result by 0·8, the model and MD correlation functions become virtually indistinguishable.

In summary, we have shown that the apparent time course of the Met36 angular reorientational correlation function is not statistically meaningful. Apart from the initial ultrafast decay, the shape of this correlation function results from a single large amplitude reorientational transition that, by chance, occurred at 270 ps. Similar artefactual correlation functions have been obtained from MD simulations of the reorientational dynamics of tryptophan residues in proteins (see, e.g. Harris & Hudson, 1991). The reorientational correlation time (or equivalently, the rate) of this transition cannot be determined from the trajectory. Since, however,

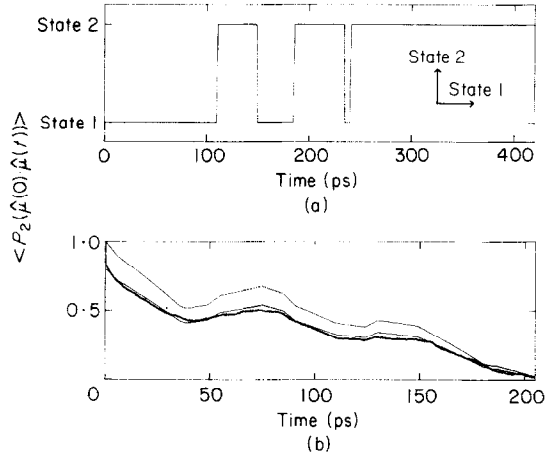

Figure 11. Comparison of the angular reorientational correlation function, $\langle P_2(\hat{\mu}(0)\cdot\hat{\mu}(t))\rangle$, for Gly33 calculated from the MD simulation (thick line with "noise" (b)) with that (thin line starting at 1·0, (b)) calculated from the model trajectory shown in (a). This trajectory depicts 5 transitions between states 1 and 2 occurring between 100 and 250 ps, which reorient the N–H vector by ~90°. When the resulting correlation function is scaled by 0·8 to allow for ultrafast librational motion in the 2 states, it becomes very similar to the result calculated from the full MD trajectory.

only one transition is observed in 420 ps, it is likely that it is not in the extreme narrowing limit. Thus, jumps between hydrogen-bonded loop conformations in which the N–H bonds have well-defined orientations are likely candidates for the slow internal motions that have been inferred from ^{15}N relaxation experiments.

As another example of the above analysis, consider the dynamics of the N–H bond of Gly33, which is also a class 2 residue in loop 1. The reorientational correlation function of this bond, calculated from the MD simulation, is shown in Figure 11 as the thick line with "noise" in the bottom panel. The motion of this bond results from several dihedral transitions that occur during the trajectory, as can be seen from the time course of the backbone ϕ torsion angle of Gly33 in Figure 5. The end result of these transitions is to reorient the N–H vector between two states with $\delta = 90°$. This is represented in Figure 11(a), where it is assumed that the jumps between the two states occur simultaneously with the dihedral transitions of ϕ(33) in Figure 5. Using this model trajectory in equation (2), gives the line starting out at 1·0 shown in Figure 11(b). When this result is scaled by 0·8, to allow for ultrafast librational motion in the two states, the agreement with the correlation function from the full MD simulation becomes remarkably good. Thus the shape of the MD correlation function is a reflection of the random times at which transitions between the two states occurred. These transitions were too infrequent to yield a statistically meaningful correlation function.

(f) *Concluding remarks*

The 500 ps MD simulation of IL-1β in water presented in this paper shows that the majority of backbone N–H bonds undergo fast librational motion with relatively small amplitude ($S^2 \sim 0{\cdot}8$) in agreement with ^{15}N n.m.r. relaxation experiments. In addition, two different types of large amplitude fluctuations are observed in the MD simulation.

First, in loop 3, which has no specific secondary structure in the simulation, the N–H vectors assume a large number of different orientations on the 10 to 50 ps time-scale (e.g. Gly140 in Figs 6 and 9). The simplest model consistent with this behaviour is motion in a cone with a substantial semiangle. The predicted flexibility of this loop, while consistent with X-ray temperature factors, is not reflected in the n.m.r. relaxation data.

A different kind of large amplitude motion is seen in loop 1 (e.g. Gly33 and Met36 in Figs 5, 10, and 11). Here, infrequent dihedral angle transitions occur, breaking some hydrogen bonds and forming others, thus preserving the structure of the loop. The overall result is that the N–H vectors jump between two states. In each of these states, there is a small spread in orientation due to fast librational motion. We have seen that this picture is quantitatively consistent with the reorientational correlation functions calculated from the MD simulation. The apparent decay of these functions, however, is not statistically meaningful, as only a few transitions are seen during the course of the MD trajectory. Clearly a 500 ps trajectory cannot be used to establish the rate of processes that occur on a comparable time-scale. Nevertheless, the present trajectory was long enough to contain several large amplitude transitions between conformations stabilized by hydrogen bonds, suggesting that these represent the physical basis for the slow motions that have been inferred from ^{15}N n.m.r. relaxation experiments.

Helpful discussions with Richard W. Pastor are gratefully acknowledged. We thank Peter J. Steinbach for supplying one of the programs used to fit the correlation functions. This work was supported by the Intramural AIDS Targeted Antiviral Program of the Office of the Director of the National Institutes of Health (to G.M.C., A.M.G. and B.R.B.).

References

Allen, M. P. & Tildesley, D. J. (1987). *Computer Simulation of Liquids*, Clarendon Press, Oxford.

Artymiuk, P. J., Blake, C. C. F., Grace, D. E. P., Oatley, S. J., Phillips, D. C. & Sternberg, M. J. (1979). Crystallographic studies of the dynamic properties of lysozyme. *Nature (London)*, **280**, 563–568.

Bernstein, F. C., Koetzle, T. F., Williams, G. J. B., Meyer, E. F., Jr, Brice, M. D., Rodgers, J. R., Kennard, O., Shimanouchi, T. & Tasumi, M. (1977). The protein data bank: a computer-based archival file for macromolecular structures. *J. Mol. Biol.* **112**, 535–542.

Brooks, B. R. (1987). Application of molecular dynamics for structural analysis of proteins and peptides. In

Super Computer Research in Chemistry and Chemical Engineering. ACS Symp. Ser. 353 (Jensen, K. F. & Truhlar, D. G., eds), pp. 123–145, American Chemical Society, Washington DC.

Brooks, B. R., Bruccoleri, R. E., Olafson, B. D., States, D. J., Swaminathan, S. & Karplus, M. (1983). CHARMM: a program for macromolecular energy, minimization, and dynamics calculations. *J. Comp. Chem.* **4**, 187–217.

Brooks, C. L., Karplus, M. & Pettitt, B. M. (1988). *Proteins: A Theoretical Perspective of Dynamics, Structure and Thermodynamics*, John Wiley & Sons, Inc.

Brünger, A. & Karplus, M. (1988). Polar hydrogen positions in proteins: empirical energy placement and neutron diffraction comparison. *Proteins Struct., Funct. Genet.* **4**, 148–156.

Clore, G. M. & Gronenborn, A. M. (1991). Comparison of the solution nuclear magnetic resonance and X-ray crystal structures of human recombinant interleukin-1β. *J. Mol. Biol.* **221**, 47–53.

Clore, G. M., Driscoll, P. C., Wingfield, P. T. & Gronenborn, A. M. (1990*a*). Analysis of the backbone dynamics of interleukin-1β using two-dimensional inverse detected heteronuclear ^{15}N–^{1}H NMR spectroscopy. *Biochemistry*, **29**, 7387–7401.

Clore, G. M., Szabo, A., Bax, A., Kay, L. E., Driscoll, P. C. & Gronenborn, A. M. (1990*b*). Deviation from the simple two-parameter model-free approach to the interpretation of nitrogen-15 nuclear magnetic relaxation of proteins. *J. Amer. Chem. Soc.* **112**, 4989–4991.

Clore, G. M., Bax, A., Wingfield, P. T. & Gronenborn, A. M. (1990*c*). Identification and localization of bound internal waters in the solution structure of interleukin-1β by heteronuclear three-dimensional ^{1}H rotating frame overhauser ^{15}N–^{1}H multiple quantum coherence NMR spectroscopy. *Biochemistry*, **19**, 5671–5676.

Clore, G. M., Wingfield, P. T. & Gronenborn, A. M. (1991). High-resolution three-dimensional structure of interleukin 1β in solution by three- and four-dimensional nuclear magnetic resonance spectroscopy. *Biochemistry*, **30**, 2315–2323.

Dinarello, C. A. & Savage, N. (1989). Interleukin-1 and its receptor. *CRC Crit. Rev. Immunol.* **9**, 1–20.

Driscoll, P. C., Gronenborn, A. M., Wingfield, P. T. & Clore, G. M. (1990). Determination of the secondary structure and molecular topology of interleukin-1β by use of two and three-dimensional heteronuclear ^{15}N–^{1}H NMR spectroscopy. *Biochemistry*, **29**, 4668–4682.

Finzel, B. C., Clancy, L. L., Holland, D. R., Muchmore, S. W., Watenpaugh, K. D. & Einspahr, H. M. (1989). Crystal structure of recombinant human interleukin-1β at 2·0 Å resolution. *J. Mol. Biol.* **209**, 779–791.

Fraunfelder, H., Petsko, G. A. & Tsernoglou, D. (1979). Temperature-dependent X-ray diffraction as a probe of protein structural dynamics. *Nature (London)*, **280**, 558–563.

Harris, D. L. & Hudson, B. S. (1991). Fluorescence and molecular dynamics study of the internal motions of the buried tryptophan in bacteriophage T4 lysozyme. *Chem. Phys.* **158**, 353–382.

Hartmann, H., Parak, F., Steigemann, W., Petsko, G. A., Ringe Ponzi, D. & Fraunfelder, H. (1982). Conformational substrates in a protein: structure and dynamics of metmyoglobin at 80 K. *Proc. Nat. Acad. Sci., U.S.A.* **79**, 4967–4971.

Ichiye, T. & Karplus, M. (1987). Anisotropy and anharmonicity of atomic fluctuations in proteins: analysis of a molecular dynamics simulation. *Proteins*, **2**, 236–259.

Jorgensen, W. L., Chandrasekhar, J., Medura, J. D., Impey, R. W. & Klein, M. L. (1983). Comparison of simple potential functions for simulating water. *J. Chem. Phys.* **79**, 926–935.

Karplus, M. & McCammon, J. A. (1983). Dynamics of proteins: elements and function. *Annu. Rev. Biochem.* **52**, 263–300.

Lipari, G. & Szabo, A. (1982*a*). Model-free approach to the interpretation of nuclear magnetic resonance relaxation in macromolecules. 1. Theory and range of validity. *J. Amer. Chem. Soc.* **104**, 4546–4559.

Lipari, G. & Szabo, A. (1982*b*). Model-free approach to the interpretation of nuclear magnetic resonance relaxation in macromolecules. 2. Analysis of experimental results. *J. Amer. Chem. Soc.* **104**, 4559–4570.

Lipari, G., Szabo, A. & Levy, R. M. (1982). Protein dynamics and NMR relaxation: comparison of simulations with experiment. *Nature (London)*, **300**, 197–198.

Lee, B. & Richards, F. M. (1971). Interpretation of protein structures: estimation of static accessibility. *J. Mol. Biol.* **55**, 379–400.

Levitt, M. (1983). Molecular dynamics of native protein. I. Analysis and nature of motion. *J. Mol. Biol.* **168**, 621–657.

Levy, R. M., Karplus, M. & McCammon, J. A. (1981). Increase of ^{13}C NMR relaxation times in proteins due to picosecond motional averaging. *J. Amer. Chem. Soc.* **103**, 994–996.

Loncharich, R. J. & Brooks, B. R. (1989). The effects of truncating long-range forces on protein dynamics. *Proteins Struct., Funct. Genet.* **6**, 32–45.

Loncharich, R. J. & Brooks, B. R. (1990). Temperature dependence of dynamics of hydrated myoglobin. *J. Mol. Biol.* **215**, 439–455.

London, R. E. (1980). Intramolecular dynamics of proteins and peptides as monitored by nuclear magnetic relaxation experiments. In *Magnetic Resonance in Biology*, (Cohen, J. S., ed.), vol. 1, pp. 1–69, Wiley, New York.

McCammon, J. A., Gelin, B. R. & Karplus, M. (1977). Dynamics of folded proteins. *Nature (London)*, **267**, 585–590.

Oppenheim, J. J., Kovacs, E. J., Matsushima, K. & Durum, S. K. (1986). There is more than one interleukin 1. *Immunol. Today*, **7**, 45–56.

Pastor, R. W. (1992). Techniques and applications of langevin dynamics simulations. In *The Molecular Dynamics of Liquid Crystals* (Luckhurst, G. R., ed.), Kluwer Academic Publishers, The Netherlands, in the press.

Post, C. B., Brooks, B. R., Dobson, C. M., Artymiuk, P., Cheetham, J., Phillips, D. C. & Karplus, M. (1986). Molecular dynamics simulations of native and substrate-bound lysozyme: a study of the average structures and atomic fluctuations. *J. Mol. Biol.* **190**, 455–479.

Priestle, J. P., Schar, H.-P. & Grutter, M. G. (1989). Crystallographic refinement of interleukin-1β at 2·0 Å resolution. *Proc. Nat. Acad. Sci., U.S.A.* **86**, 9667–9671.

Reiher, W. E. (1985). Theoretical studies of hydrogen bonding. Ph.D. thesis, Harvard University, Cambridge, M.A.

Shrake, A. & Rupley, J. A. (1973). Environment and exposure to solvent of protein atoms: lysozyme and insulin. *J. Mol. Biol.* **79**, 351–371.

Sternberg, M. J. E., Grace, D. E. P. & Phillips, D. C. (1979). Dynamic Information from protein crystallography: an analysis of temperature factors from refinement of the hen egg-white lysozyme structure. *J. Mol. Biol.* **130**, 231–253.

Tainer, J. A., Getzoff, E., Alexander, J., Houghton, R. A., Olson, A. J., Lerner, R. A. & Hendrickson, W. A. (1984). The reactivity of anti-peptide antibodies is a function of the atomic mobility sites in a protein. *Nature (London)*, **312**, 127–134.

Veerapandian, B., Gilliland, G. L., Raag, R., Svensson, A. L., Masui, Y., Hirai, Y. & Poulos, T. L. (1992). Functional implications of interleukin-1β based on the three-dimensional structure. *Proteins, Struct., Funct. Genet.* **12**, 10–23.

Westhoff, E., Altschu, D., Moras, D., Bloomer, A. C., Mondragon, A., Klug, A. & van Regenmortel, M. H. V. (1984). Correlation between segmental mobility and the location of antigenic determinants in proteins. *Nature (London)*, **311**, 123–126.

Zwanzig, R. & Ailawadi, N. K. (1969). Statistical error due to finite time averaging in computer experiments. *Phys. Rev.* **182**, 280–283.

Edited by P. E. Wright